Scientific Research Publishing

World Journal of Engineering and Technology, 2023, 11, 136-152
https://www.scirp.org/journal/wjet
ISSN Online: 2331-4249
ISSN Print: 2331-4222

An Investigation of the Effects of Thermal Interference between Adjacent Nitinol Spring Actuators in a Tactile Display

Kudzanai Sekerere[1*], Rehema Ndeda[2], Karanja Kabini[2]

[1]Department of Mechatronic Engineering, Pan African University Institute for Basic Sciences, Technology and Innovation, Juja Town, Kenya
[2]Department of Mechatronic Engineering, Jomo Kenyatta University of Agriculture and Technology, Juja Town, Kenya
Email: *sekerere.kudzanai@students.jkuat.ac.ke

How to cite this paper: Sekerere, K., Ndeda, R. and Kabini, K. (2023) An Investigation of the Effects of Thermal Interference between Adjacent Nitinol Spring Actuators in a Tactile Display. *World Journal of Engineering and Technology*, **11**, 136-152.
https://doi.org/10.4236/wjet.2023.111010

Received: August 15, 2022
Accepted: February 25, 2023
Published: February 28, 2023

Abstract

Over the years, there has been increased research interest in the application of Nitinol as an actuator, due to its shape memory behaviour, simplicity, high power-to-weight ratio, compactness, and extreme high fatigue resistance to cyclic motion, and noiseless operation. Nitinol has found application in tactile displays which reproduce tactile parameters such as texture and shape, depending on the application. This paper presents the effects of thermal interference between adjacent Nitinol spring actuators in a tactile display. The tactile display is made of a 3 by 3 pin array whose spatial resolution was varied from 4 mm to 6 mm in steps of 1 mm while a current of 1.5 A was used to actuate 8 of the springs, and the centre spring was left unactivated to observe the thermal effects on it due to the heat gradient formed. A Finite Element (FE) model was developed using COMSOL Multiphysics and the results were further verified through experimentation. In both cases, there was visible thermal interference between actuators. The increase in spatial resolution saw a decrease in thermal interference by 12.7%. Using a fan to introduce forced convection, reduced the thermal interference in the simulation by 20% and during experimentation by 11%. The results of this research indicate a spatial resolution of 6 mm reduced the thermal inference to a negligible rate. However, thermal interference could not be eliminated with these two methods.

Keywords

Finite Element Analysis (FEA), Shape Memory Alloy (SMA), Nitinol (NiTi) Spring Actuator, Tactile Display, Thermal Interference

1. Introduction

Rapid development in the field of virtual reality (VR) and associated technologies has recently sprouted considerable research interest in tactile displays [1]. Tactile sensation is one of the principal sensory functions in the human body, specifically, the information received corresponding to varying vibrations and pressure against the skin [2]. A tactile display is an intelligent device that can mimic several physical modalities depending on the application, such as texture, temperature, shape, position and motion [3]. Compact tactile display devices have been suggested for use as an interface in minimal inverse surgery, remote real-time surgery systems [4], virtual environment (VE) applications, aerospace systems, braille devices for the blind, as tactile communication in mobile environments, and as a substitution/complement of the visual presentation of information [5].

Several innovative materials already in use in other fields and products have been re-designed for tactile display actuation such as: electromagnetic linear actuators [6], piezo elements [7], rheological materials [8] and shape memory alloy (SMA) materials [9]. Shape Memory Alloys (SMAs) are exceptional smart materials with properties of pseudoelasticity (PE) and shape memory effect (SME) due to their thermomechanical characteristics and phase transformations [10]. SMAs fulfil several important characteristics; in particular, they are lightweight, have a high energy density, reduced power to weight ratio [11], and extremely high fatigue resistance to cyclic motion, compactness [12] and noiseless operation [1]. SMAs have found applications as sensors and actuators in several industries including aerospace, biomedicine [13], and robotics. A variety of SMAs are available in the market though the most used is a nickel-titanium alloy best known as Nitinol (NiTi). Nitinol elements with a desirable shape are fabricated from elementary products such as bars, ribbons, wires and sheets into products such as hooks, springs, and washers.

A tactile display is made up of several tactile elements or taxels. The number of taxels is highly dependent on the application and desired size of the display. The distance between each taxel is determined by the two-point discrimination threshold (TPDT), in human fingertips, which is 1.5 - 3 mm, thus for most tactile displays this is the minimum taxel separation [14]. NiTi is favoured as an actuator for a tactile display due to its relatively large displacement and high actuating force in space-constrained applications; this is in comparison to other actuators of a similar size [2]. The SME phenomena in NiTi are influenced by the fabrication process, a combination of annealing at a specific temperature, cold work and post-heat treatment, comprehensively determining its characteristics. In this work, NiTi helical springs were utilized as taxel actuators. NiTi helical springs are monolithic SMA actuators that can be used to mimic antagonistic motion using applied stress or temperature-induced phase transformation that results in stretching/contraction motion. During phase transformation, the NiTi material changes its phase state from twinned martensite to austentite [15],

while developing a corresponding SME-driven motion.

A tactile sensor measures the parameter value of interest [16] and sends a signal to the system controller which converts it to a signal passed to the tactile display through the NiTi driving circuit, which sends a current equivalent to the desired actuation to the NiTi springs. This current causes resistive heating in the NiTi spring actuators that in turn causes the phase transformation resulting in the driving motion. Depending on the information displayed, several taxel actuators will be simultaneously actuated at varying intervals. Each taxel actuator will increase in temperature and some of that heat will be lost to the surrounding environment. The thermal effect of the radiated heat on adjacent taxel actuators may cause some distortion to the displayed information. Though there has been increased research on the use of NiTi as an actuator, the focus has been placed on finding the best method of control due to its non-linear behaviour [3] [17] [18]. The thermal effects on adjacent taxel actuators when NiTi is used have not been researched much. A few researchers have glimpsed the evidence of thermal interference between adjacent NiTi actuators but there has not been an investigation into the effects as the researchers were focusing on the control element [2] [19] [20]. Thus, the focus of this paper shall be solemnly on investigating the effects of the thermal radiation between adjacent NiTi taxel actuators in a Tactile Display. A 3 × 3 tactile display is utilized for this investigation.

2. Materials and Methods

2.1. Tactile Display Design

The tactile display device is designed using the concept introduced by Mansour [21]. It is a 3 × 3 taxel matrix designed to present both shape and stiffness information. Considering the TPDT and the mean coil diameter of the springs used being 3.45 mm; the spatial resolution was varied from 4 mm to 6 mm in steps of 1 mm. **Figure 1** is a CAD MODEL of the tactile display, while **Figure 2** shows the structure of the taxel. Each taxel unit utilizes two decoupled NiTi springs; the upper springs are responsible for displaying the object's shape by change in their vertical displacement, known as the elongation springs (ES). The lower springs are responsible for displaying object stiffness by changing the rate of compressive force applied against the taxel and they are known as the stiffness springs (SS). The ES and SS are in series on a single taxel so that the user can simultaneously feel the resultant change in object shape and stiffness. The behaviour of the springs is dependent on their change in phase when heating occurs due to the eddy current formed when a current is applied. In this research focus was placed on the ES. The displacement of the ES occurs due to the application of an electrical current that induces a temperature increase that causes the change of phase and allows for a maximum stroke of 10 mm. Though precision control of the extent of the stroke is possible, this research only considered the spring in full stroke position and when unactivated; thus, it only applied an on/off control mechanism. The ES follows the principle of the two-way shape

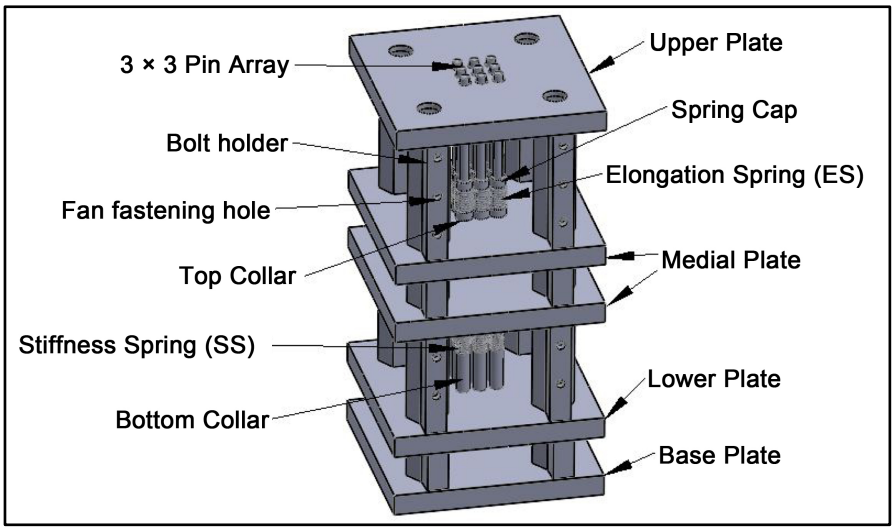

Figure 1. Tactile display structure.

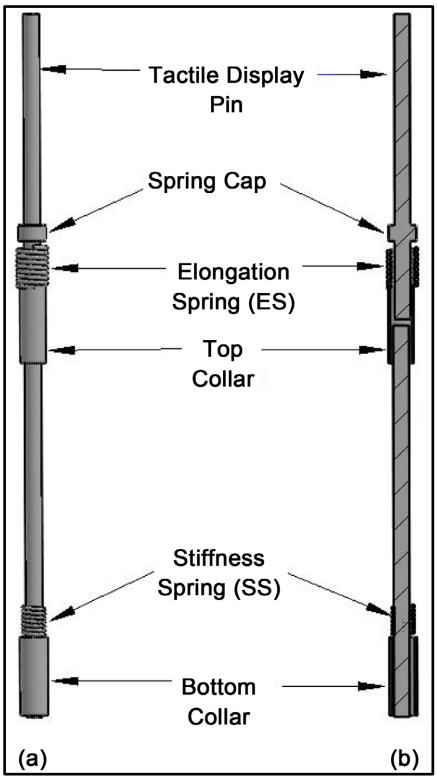

Figure 2. (a) Tactile pin structure; (b) Cross-sectional view of the tactile pin.

memory effect [22] to present object shape by displacing the taxel to a certain height depending on the amount of austenite phase transformation and retaining its shape when cooled back to the martensite state. The taxel is prevented from moving beyond the prescribed range by the spring cap when it has contact with the upper plate. The top and bottom collar help keep the pin from wambling during it's displacement. The top collar is held into place by the medial

plates, while the bottom collar is held in place by the lower plate. The tactile display structure is held together by 4 bolts going through each plate and the bolt holders act as a means of keeping the desired spacing in between the plates. The bolt holders were also used to fasten the cooling fans on to the structure. A single cooling fan was fastened on the bolt holders in between the medial and upper plate. The total height of the tactile display structure is 10 cm, while the plates have a length and width of 50 mm each and a 5 mm thickness. The height between the medial and upper plate was 30 mm.

2.2. System Design

A summarized description of the system architecture is included in this paper, since the full control design description is outside of the scope of this paper. Figure 3 shows the layout of the system. An open loop system was used for actuating the NiTi springs. A 3 × 3 tactile array was fabricated utilizing a combination of 3D printing and laser cutting. Perspex was used as the upper plate of the tactile structure to allow for thermal imaging of the NiTi actuators. The thermal imaging camera used was the Seek Thermal Compact imaging camera, with a 206 × 156 thermal sensor and a 36˚ field of range focusable camera was used to evaluate the thermal interference instead of attaching thermocouples to the NiTi springs to reduce the strain exerted on them. A LabVIEW program was used to send the control signal and receive sensor feedback through an Arduino board. The SMA driving circuit received signals from the Arduino board to actuate the springs and the INA219 current sensors were used to evaluate that the sent signal is equivalent to the value received by the springs. A 5 Volt electronics cooling fan with a speed of 8000 rpm and an induced airflow of 2 cfm was used to produce the forced convection environment. A power supply with a rating of 30 VDC and 15A was used.

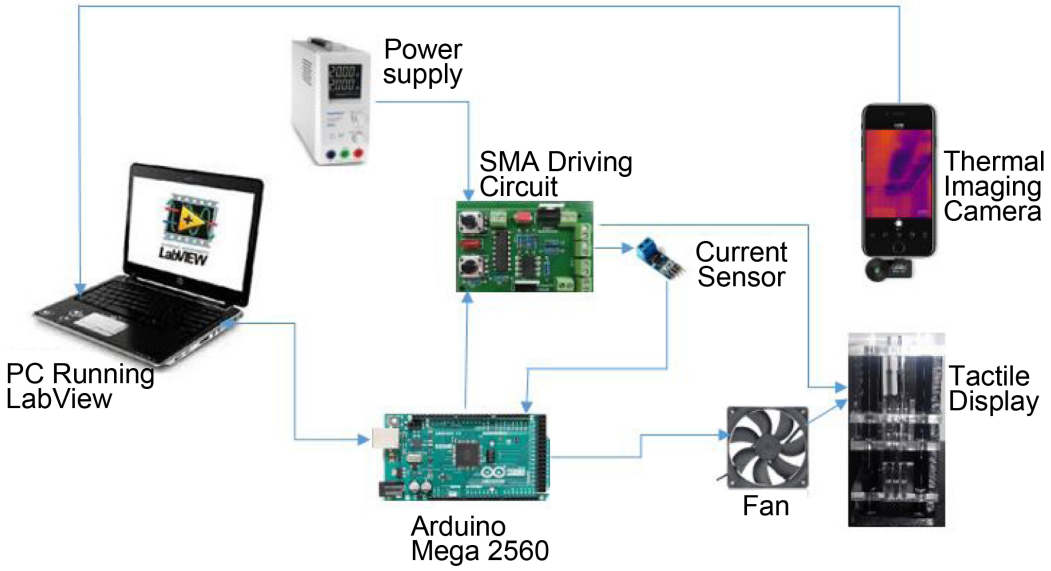

Figure 3. System setup.

3. NiTi SMA Thermal Dynamics

A NiTi SMA actuator is heated by applying an electric current across it through a process of resistive (joule) heating [23] [24]. The movement of the NiTi actuator is highly dependent on its temperature, an increase in temperature results in an equivalent increase in the material's young's modulus. Thus with increased temperature, the force exerted by a NiTi element increases dramatically [25]. Consequently, to determine the dynamic response of the actuator the transformation temperatures have to be known. In this work, NiTi SMA springs known by the trade name Flexinol which are manufactured by Dynalloy Inc. were used. The Flexinol parameters used for both finite element analysis (FEA) and the experiments were taken from the manufacturer technical data sheets [26] and literature [27] [28] are as shown in **Table 1**.

The thermal equilibrium is such that the stored energy of the system is equivalent to the rate of heat transfer. Thermal energy is introduced into the system through joule heating and lost through natural convection. The system's stored energy comprises latent heat and internal energy. This can be represented mathematically by [9] [29]:

$$\rho V\left[\underbrace{C_p\frac{\mathrm{d}T}{\mathrm{d}t}}_{\text{internal energy}}+\underbrace{\Delta H\frac{\mathrm{d}\zeta}{\mathrm{d}t}}_{\text{latent heat}}\right]=\underbrace{Ri^2}_{\text{joule heating}}-\underbrace{hS\left(T-T_\infty\right)}_{\text{natural convection}} \tag{1}$$

Table 1. Flexinol parameters.

Parameters	Phase	Value	Unit
Transformation Temperatures	Martensite (M_f, M_s)	68, 78	˚C
	Austenite (A_f, A_s)	88, 98	
Thermal Conductivity (k)	Martensite	8	W/(m ˚C)
	Austenite	18	
Coefficient of thermal expansion (α)	Martensite	6.6×10^{-6}	1/˚C
	Austenite	11×10^{-6}	
Specific Heat (C_p)		840	J/(kg ˚C)
Density (ρ)		6450	kg/m^3
Electrical Resistivity	Martensite	80×10^{-8}	Ωm
	Austenite	100×10^{-8}	
Resistivity temperature coefficient	Martensite	1.94×10^{-4}	1/˚C
	Austenite	5.07×10^{-4}	
Young's Modulus (E)	Martensite (E_M)	28 - 41	GPa
	Austenite (E_A)	75 - 83	
Resistance		50	Ω
Emissivity		0.4	
Poison's Ratio		0.33	

where ρ is the density of the NiTi, V is the volume of the material, C_p is the specific heat capacity of NiTi spring material, ΔH is the latent heat of phase transformation, R is the electrical resistance of the wire, i is the heating current supplied by the source, h is the heat-transfer coefficient for the system, S is the exposed surface area of the NiTi, $\frac{\mathrm{d}\zeta}{\mathrm{d}t}$ is the phase transformation term and T_∞ is the ambient temperature.

If a resistive current is applied to the NiTi spring and it reaches a steady state temperature at the austenitic finish phase, with a small distance between adjacent taxels, the taxels' thermal state is influenced by the heat gradient. A two-dimensional (2D) heat transfer problem occurs within the tactile array that can be described mathematically by utilizing Fourier's steady state heat flow rate as [20]:

$$Q(t) = kS\nabla T \tag{2}$$

where Q is the flow rate of the heat convection away from the NiTi spring actuator, k is the atmospheric thermal conductivity ($k = 0.025\ \mathrm{W/m \cdot K}$), and ∇T is the temperature gradient at the area of interest. An assumption that Q is consistent within the SMA area S is made [20].

4. Simulation and Experimental Results

The 3 × 3 NiTi spring array was simulated in COMSOL Multiphysics software to analyze the heat transfer dynamics between the adjacent springs. The distance of separation was varied from 4 - 6 mm in step intervals of 1 mm. The distance of separation was determined by factoring in the two-point discrimination threshold which is between 1.5 - 3 mm for spatial acuity in fingertips [30]. The springs used for the simulation and experiments had a wire diameter of 0.8 mm, a mean diameter of 3.45 mm and 10 number of turns. The rated current of 1.5 A was passed through 8 springs fully actuating them and reaching temperatures above austenite finish temperature, while 1 spring in the central position was left without any current passing through it, to visualize the impact of the temperature gradient formed by the heat from the actuated springs on the unactuated spring [19]. The simulation utilized the material parameters listed in **Table 1**, and it was set such that the springs are simulated in an environment such is that of a laboratory with a room temperature of 20˚C and normal air pressure. The simulation geometry only included the upper plate, the medial plate and the elongation springs between them. The change in temperature was measured on the surface of the springs. The simulation is conducted for the varying spatial resolution within a normal convection environment and forced convection from a simulated fan. The fan was set up to mimic the parameters of a fan used in small electronic devices with 8000 rpm and airflow of 2 cfm. The varying from normal to forced convection helped reduce the thermal interference between the adjacent springs. A graph of temperature against time was plotted for all 9 springs. Similar spatial resolution and current utilized in the simulation model

were used in the experiments to validate the results.

Figures 4-6 show graphs of the simulation at a spatial resolution of 4, 5 and 6 mm respectively. Figure 4(a) shows the spring's temperature rise under normal convection. The 8 actuated springs rise to a temperature of 105˚C and the temperature of the unactuated spring rises to 52˚C. Figure 4(b) shows the spring's temperature rise under forced convection. The 8 actuated springs rise to a temperature of 105˚C and the temperature of the unactuated spring temperature rises to 42˚C. There is a 20% drop in temperature rise for the unactuated spring within a forced convection environment.

Figure 5 shows graphs of the simulation at a spatial resolution of 5 mm. Figure 5(a) shows the temperature of the unactuated spring rises to 45˚C under normal convection, which is 10% less than at a spatial resolution of 4 mm. Figure 5(b) shows the temperature of the unactuated spring rises to 35˚C under forced convection. There is a 22% drop in the temperature rise of the unactuated

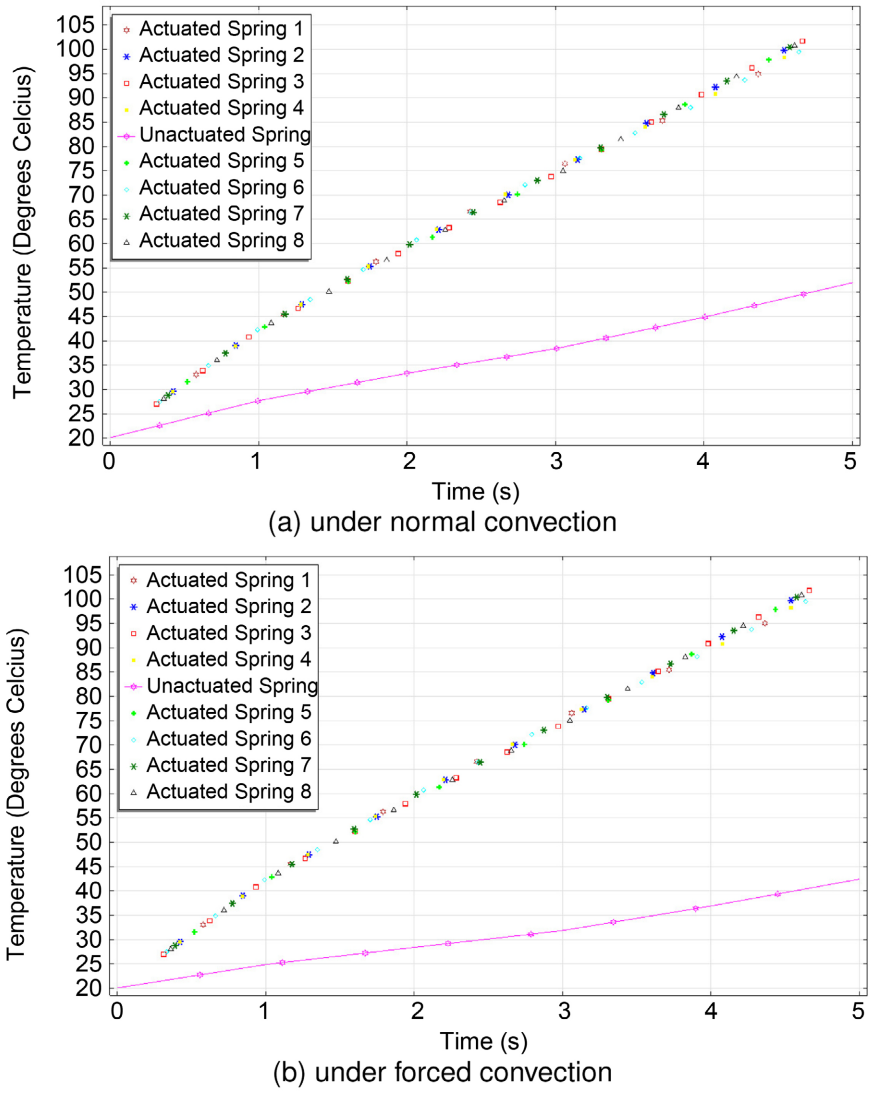

Figure 4. Increase in temperature for springs with a 4 mm spatial resolution.

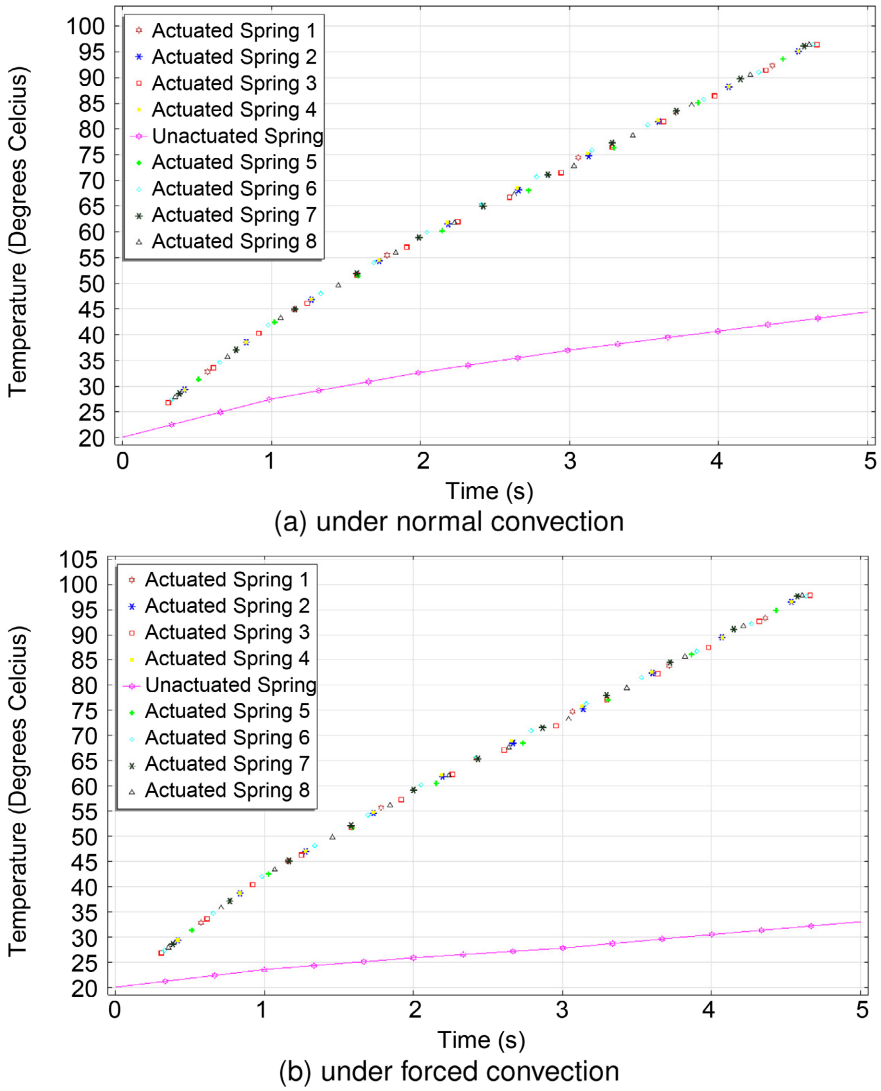

Figure 5. Increase in temperature for springs with a 5 mm spatial resolution.

spring within a forced convection environment.

Figure 6 shows graphs of the simulation at a spatial resolution of 6 mm. **Figure 5(a)** shows the temperature of the unactuated spring rises to 40˚C under normal convection, which is 20% less than at a spatial resolution of 4 mm and 11% less than at a spatial resolution of 5 mm. **Figure 5(b)** shows the spring's temperature rise under forced convection. The temperature of the unactuated spring rises to 31˚C. There is a 25% drop in the temperature rise of the unactuated spring within a forced convection environment.

Figure 7 shows the rise in temperature of the unactuated spring at the different spatial resolutions of 4, 5 and 6 mm. **Figure 7(a)** shows the spring under normal convection conditions, where the temperature rise reduces by 24% from 52˚C at a spatial resolution of 4 mm to 40˚C at a spatial resolution of 6 mm. **Figure 7(b)** shows the spring under forced convection, where the temperature rise reduces by 26% from 42˚C at a spatial resolution of 4 mm to 31˚C at a spatial

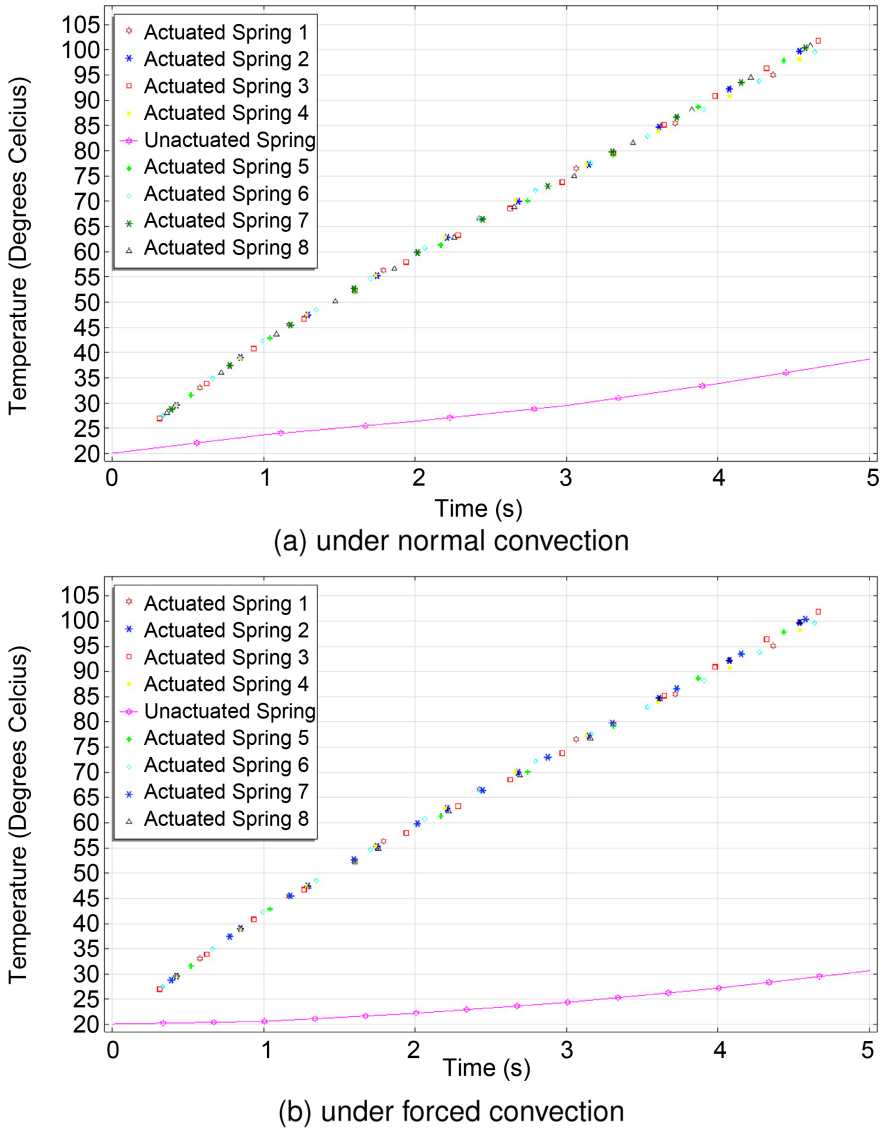

Figure 6. Increase in temperature for springs with a 6 mm spatial resolution.

resolution of 6 mm. Thus, the simulation results indicate that increasing the spatial resolution reduces the thermal interference as shown in both graphs. Furthermore, the rise in temperature of the spring is reduced by 20% under forced convection conditions in comparison to the normal convection conditions.

Figures 8-10 show thermal images of the heat maps taken of the springs during experimentation at a spatial resolution of 4, 5 and 6 mm respectively. The images were taken from a vertical view directly through the transparent upper plate of the tactile display structure with the thermal imaging camera, while the spot temperature option was selected so as to attain the temperature in the region of the unactuated spring and display the temperature on the screen. The thermal maps also covered the temperature of all the other springs from the top view, though the spot indicator was directed at the central unactuated spring. The heat radiated between the springs made it impossible to visualize the location

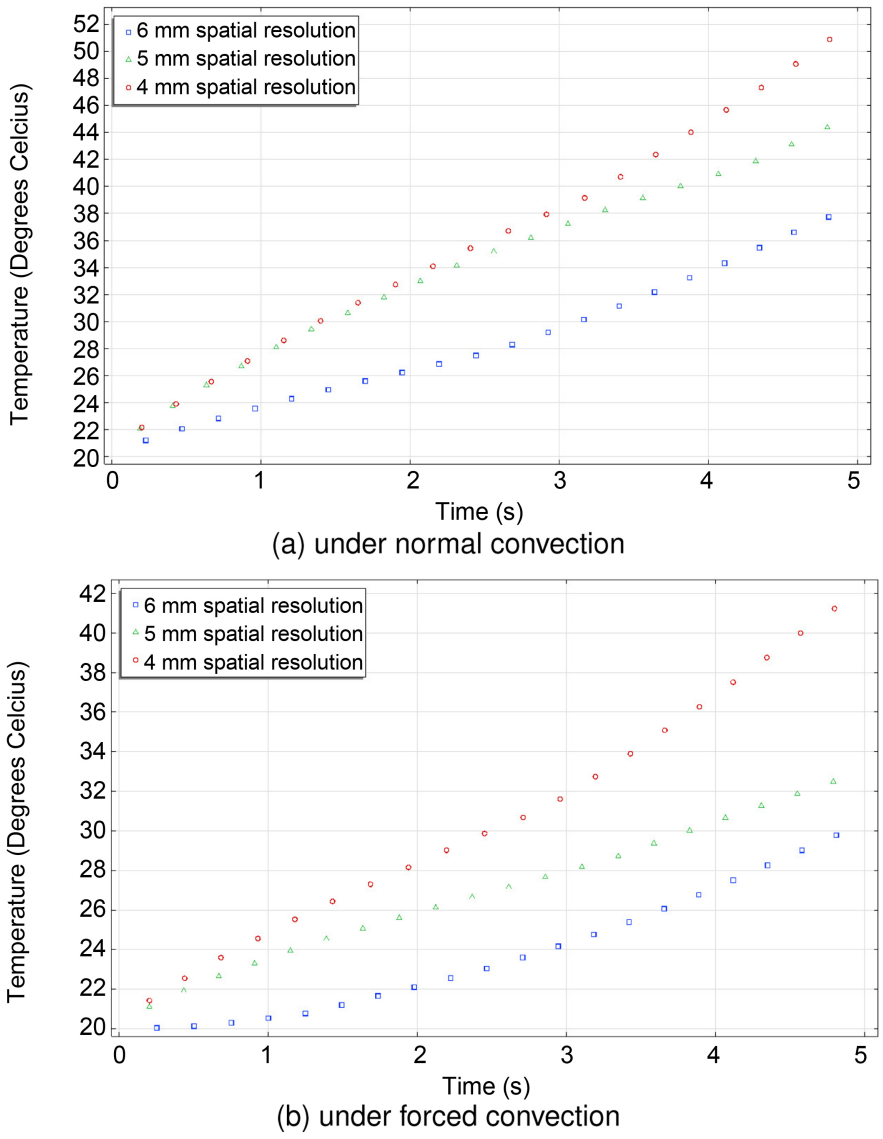

Figure 7. Increase in temperature of the unactuated springs.

of the other springs on the thermal map. **Figure 8(a)** shows the spring's temperature rise under normal convection. The 8 actuated springs rise to a temperature of about 99˚C and the temperature of the unactuated spring rises to 63˚C. **Figure 8(b)** shows the rise in temperature of the springs under forced convection. The temperature of the unactuated spring rises to 55˚C. There is a 12.7% drop in the temperature rise of the unactuated spring within a forced convection environment.

Figure 9 shows the experimental results at a spatial resolution of 5 mm. **Figure 9(a)** shows the spring's temperature rise under normal convection. The temperature of the unactuated spring rises to 57˚C, which is 9.5% less than at a spatial resolution of 4 mm. **Figure 9(b)** shows the rise in temperature of the springs under forced convection. The temperature of the unactuated spring rises to 50˚C. There is an 8.7% drop in the temperature rise of the unactuated spring

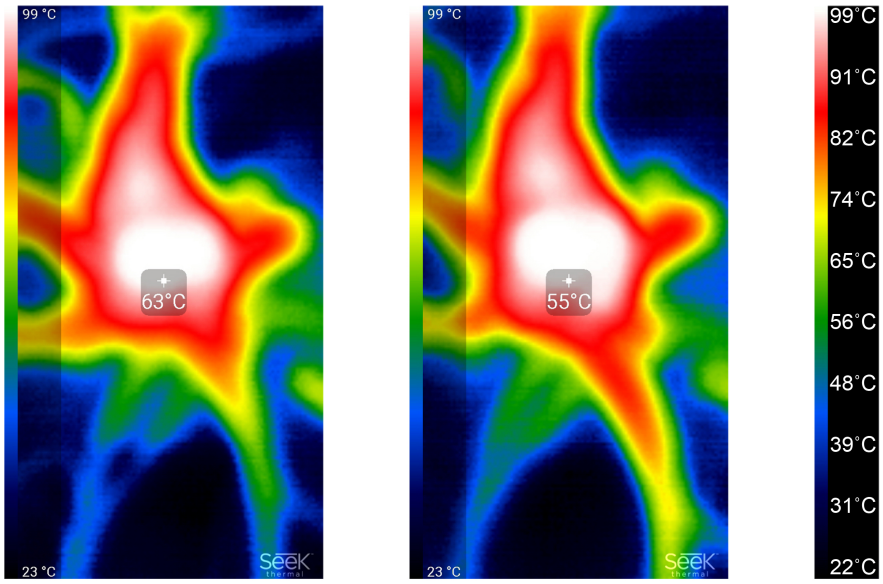

(a) under normal convection (b) under forced convection

Figure 8. Increase in temperature for springs with a 4 mm spatial resolution.

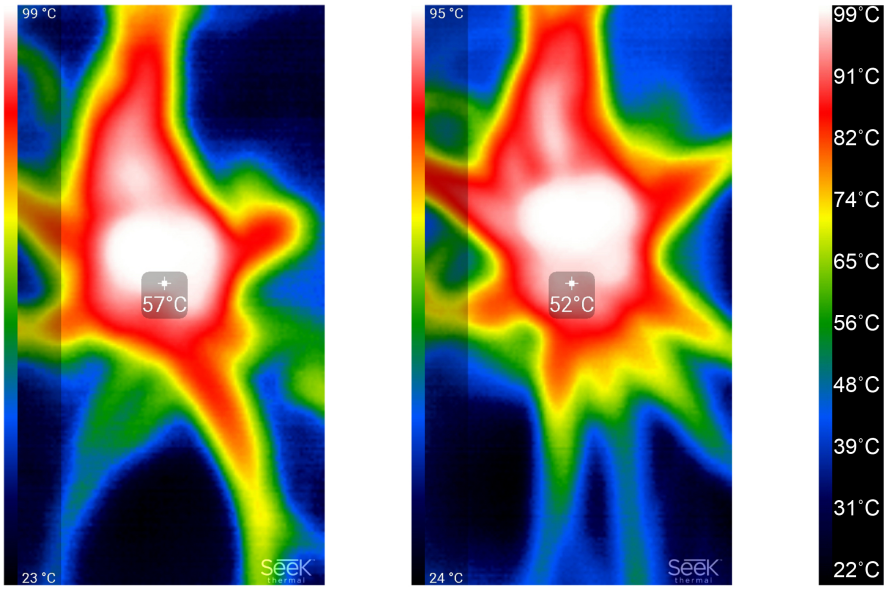

(a) under normal convection (b) under forced convection

Figure 9. Increase in temperature for springs with a 5 mm spatial resolution.

in a forced convection environment.

Figure 10 shows the experimental results at a spatial resolution of 6 mm. Figure 10(a) shows the spring's temperature rise under normal convection. The temperature of the unactuated spring rises to 55˚C, which is 12.7% less than at a spatial resolution of 4 mm. Figure 10(b) shows the rise in temperature of the springs under forced convection. The temperature of the unactuated spring rises to 49˚C. There is an 11% drop in the temperature rise of the unactuated spring within a forced convection environment.

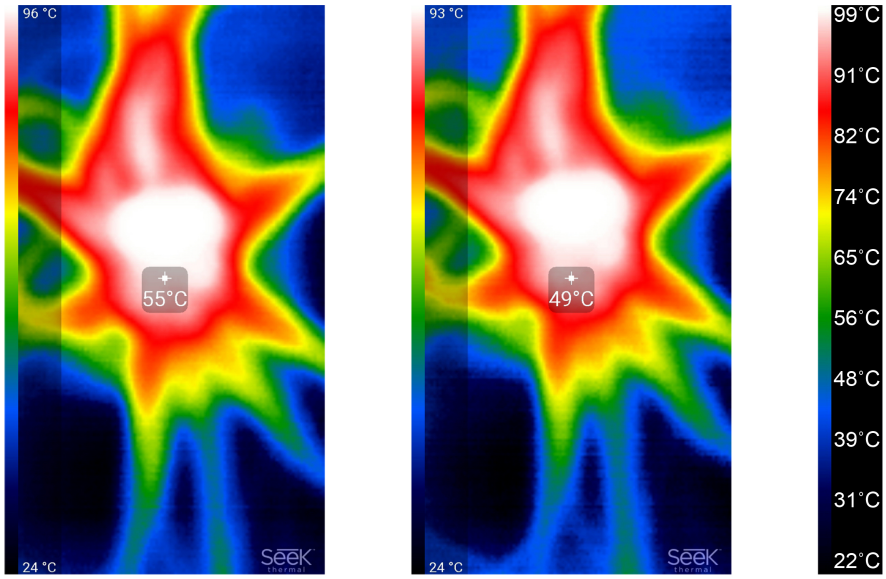

Figure 10. Increase in temperature for springs with a 6 mm spatial resolution.

The experimental results also confirm what had been noted from the simulation results, that there was definite thermal interference between adjacent nitinol springs in the tactile array. Increasing the spatial resolution under normal convection reduced the thermal interference, though there is a 20% further reduction under forced convection. There was not much deviation in the temperature of the actuated springs in the results because the heat gradient was at a maximum and the influence that the heat gradient had on the actuated springs was at a minimum due to their already high-temperature [19]. The results indicate that during the experiment at a spatial resolution of 6 mm under forced convection there was an 11% drop in the temperature rise of the unactuated spring when compared to when the spatial resolution was 4 mm. These results collaborate with the observations by Velaquez *et al.* [20], that without any cooling in a finite period the nitinol actuators would all reach a similar temperature. The simulation and experimental results indicated this happened within 30 - 60 secs. **Figure 11** shows the simulation and experimental temperature of the unactuated spring after 5 secs at a spatial resolution of 4, 5 and 6 mm. **Figure 11(a)** shows the spring temperature under natural convection, while **Figure 11(b)** shows the spring under forced convection. There was an average difference in the values of the simulation and experimental results of 26%. This difference can be attributed to the fact that the simulation utilized ideal conditions and the temperature was measured directly on the springs, whereas the experimental data was taken in a lab where the environmental conditions varied slightly with time and a thermal imaging camera was used which just highlights the external temperature on the surface of the springs. However, the experimental and simulation results indicate interference between adjacent nitinol springs within the tactile array. The use of forced convection did help reduce the extent of the thermal interference by 20%

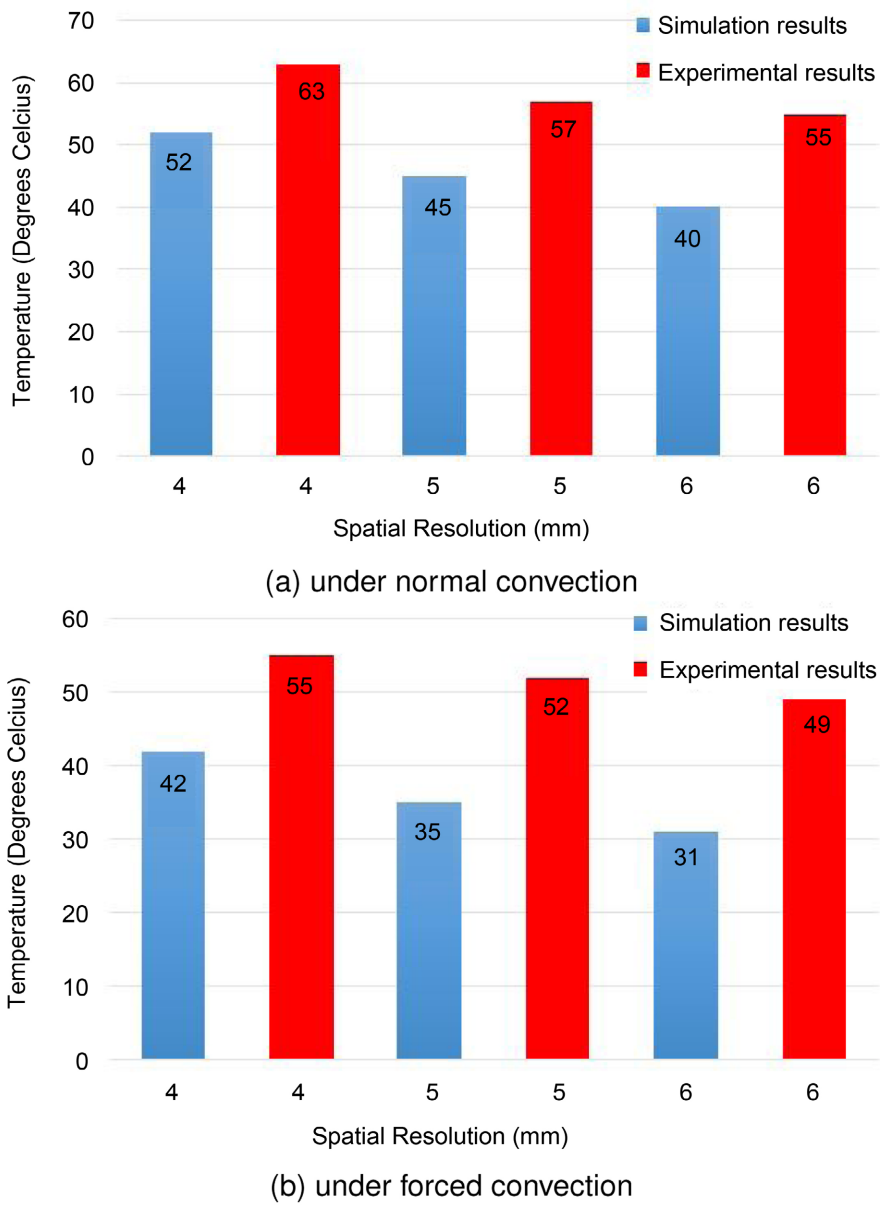

Figure 11. Increase in temperature of the unactuated springs.

following the simulation results and by 12% according to the experimental results. The spatial resolution recommended in this research was 6 mm as it reduced the thermal interference as shown by both the experimental and simulation results. However, increasing the spatial resolution did affect the overall display resolution. Thus, the displayed image might have to be displayed at a scale, while the number of taxels should be increased in proportion to the variation in the spatial resolution.

5. Conclusions

This paper has presented the effects of thermal interference between nitinol actuators within normal convection and forced convection conditions at varying

spatial resolutions. A tactile display with 9 taxels actuated by NiTi springs was designed and utilized for experimentation and a model was created to simulate the thermal behaviour of the NiTi springs. The simulation and experiments were conducted by actuating 8 of the NiTi spring actuators with a current of 1.5 A, while the central spring was left unactuated and the effects of the thermal gradient on the unactuated spring were observed.

The simulation and experiments were repeated while the spatial resolution for the tactile array was varied from 4 - 6 mm in steps of 1 mm. A thermal imaging camera was used to take thermal maps of the behaviour of the springs and the results compared to the simulation results.

It was observed that both an increase in the spatial resolution and utilizing the actuators under forced convection reduced the thermal interference between adjacent NiTi actuators. It has been recommended that the actuators be utilized under forced convection conditions as this reduces the thermal interference by 20%. A spatial resolution of 6 mm has been recommended when utilizing a spring with a coil diameter of 3.45 mm as it further reduces thermal interference between the actuators by an average of 11%. Utilizing forced convection and a spatial resolution calculated in proposition to the size of the spring limits the effects of thermal interference between the NiTi springs such that the disturbance will be negligible for the desired shape and stiffness display outcome.

Future work will evaluate other cooling methods and develop a control method that accounts for the thermal interference between the nitinol actuators. Furthermore, future work will investigate the effects of the nitinol actuator size and the tactile display array size on the thermal interference.

Acknowledgements

The first author is supported by a scholarship from the Pan African University Institute for Basic Sciences, Innovation and Technology under the commission of the African Union, which is gratefully acknowledged.

Conflicts of Interest

The authors declare no conflicts of interest regarding the publication of this paper.

References

[1] Jairakrean, S. and Chanthasopeephan, T. (2009) Position Control of SMA Actuator for 3D Tactile Display. *IEEE International Conference on Rehabilitation Robotics*, *ICORR*, Kyoto, 23-26 June 2009, 234-239. https://doi.org/10.1109/ICORR.2009.5209555

[2] Xu, J., Kimura, Y., Tsuji, K., Abe, K., Shimizu, T., Hasegawa, H. and Mineta, T. (2020) Fabrication and Characterization of SMA Film Actuator Array with Bias Spring for High-Power MEMS Tactile Display. *Microelectronic Engineering*, **227**, 111-307. https://doi.org/10.1016/j.mee.2020.111307

[3] Alsayed, Y.M., Abouelsoud, A.A. and Elbab, A.M.R.F. (2020) Adaptive PI-Based

Fuzzy Logic Auto-Tuning Controller Design and Implementation for Tactile Shape Display Device. 2019 6*th International Conference on Advanced Control Circuits and Systems* (*ACCS*) & 2019 5*th International Conference on New Paradigms in Electronics & Information Technology* (*PEIT*), Hurgada, 17-20 November 2019, 32-37. https://doi.org/10.1109/ACCS-PEIT48329.2019.9062838

[4] Yanatori, H., Mineta, T., Takeuchi, S. and Abe, K. (2016) A Shape Memory Alloy Thick Film Actuator Array for Narrow Pitched Planar Tactile Display Device. 2016 *IEEE* 11*th Annual International Conference on Nano/Micro Engineered and Molecular Systems*, Sendai, 17-20 April 2016, 251-254. https://doi.org/10.1109/NEMS.2016.7758244

[5] Chouvardas, V.G., Miliou, A.N. and Hatalis, M.K. (2008) Tactile Displays: Overview and Recent Advances. *Displays*, **29**, 185-194. https://doi.org/10.1016/j.displa.2007.07.003

[6] Wu, X., Kim, S.H., Zhu, H., Ji, C.H. and Allen, M.G. (2012) A Refreshable Braille Cell Based on Pneumatic Microbubble Actuators. *Journal of Microelectromechanical Systems*, **21**, 908-916. https://doi.org/10.1109/JMEMS.2012.2190043

[7] Velazquez, R., Pissaloux, E., Szewczyk, J. and Hafez, M. (2005) Miniature Shape Memory Alloy Actuator for Tactile Binary Information Display. *IEEE International Conference on Robotics and Automation*, Barcelona, 18-22 April 2005, 1344-1349. https://doi.org/10.1109/ROBOT.2005.1570302

[8] Leonardis, D., Claudio, L. and Frisoli, A. (2018) A Survey on Innovative Refreshable Braille Display Technologies. In: Di Bucchianico, G. and Kercher, P., eds., *AHFE* 2017: *Advances in Design for Inclusion*, Springer, Cham. https://doi.org/10.1007/978-3-319-60597-5_46

[9] Wright, C. and Bilgen, O. (2018) System Identification of a Low-Order Heat Transfer Model for Shape Memory Alloy Wires. *Journal of Intelligent Material Systems and Structures*, **29**, 2122-2136. https://doi.org/10.1177/1045389X17754260

[10] Heidari, B., Kadkhodaei, M., Barati, M. and Karimzadeh, F. (2016) Fabrication and Modeling of Shape Memory Alloy Springs. *Smart Materials and Structures*, **25**, Article ID: 125003. https://doi.org/10.1088/0964-1726/25/12/125003

[11] Emiliavaca, A., de Araújo, C., Souto, C. and Ries, A. (2019) Characterization of Shape Memory Alloy Micro-Springs for Application in Morphing Wings. *Smart Materials and Structures*, **28**, Article ID: 015010. https://doi.org/10.1088/1361-665X/aaeb80

[12] Zhang, D., Zhao, X., Han, J., Li, X. and Zhang, B. (2019) Active Modeling and Control for Shape Memory Alloy Actuators. *IEEE Access*, **7**, 162549-162558. https://doi.org/10.1109/ACCESS.2019.2936256

[13] Mansour, N.A., Fath El-Bab, A. and Abdellatif, M. (2014) Design Procedure and Simulation of a Novel Multi-Modal Tactile Display Device for Biomedical Applications. *Journal of Sensor Technology*, **4**, 7-17. https://doi.org/10.4236/jst.2014.41002

[14] Garcia-Hernandez, N., Tsagarakis, N.G. and Caldwell, D.G. (2011) Feeling through Tactile Displays: A Study on the Effect of the Array Density and Size on the Discrimination of Tactile Patterns. *IEEE Transactions on Haptics*, **4**, 100-110. https://doi.org/10.1109/TOH.2010.59

[15] Huang, W. (2002) On the Selection of Shape Memory Alloys for Actuators. *Materials and Design*, **23**, 11-19. https://doi.org/10.1016/S0261-3069(01)00039-5

[16] Fath El-Bab, A.M., Eltaib, M.E., Sallam, M.M. and Tabata, O. (2007) Tactile Sensor for Compliance Detection. *Sensors and Materials*, **19**, 165-177.

[17] Mansour, N.A., Fath El-Bab, A.M., Assal, S.F. and Tabata, O. (2015) Design, Characterization and Control of SMA Springs-Based Multi-Modal Tactile Display Device for Biomedical Applications. *Mechatronics*, **31**, 255-263. https://doi.org/10.1016/j.mechatronics.2015.08.004

[18] Awan, A.U., Park, J., Kim, H.J., Ryu, J. and Cho, M. (2016) Adaptive Control of a Shape Memory Alloy Actuator Using Neural-Network Feedforward and RISE Feedback. *International Journal of Precision Engineering and Manufacturing*, **17**, 409-418. https://doi.org/10.1007/s12541-016-0051-7

[19] Fischer, H., Trapp, R., Schüle, L. and Hoffmann, B. (1997) Actuator Array for Use in Minimally Invasive Surgery. *Journal de Physique IV*, **7**, C5-609-C5-614.

[20] Velazquez, R., Pissaloux, E.E. and Wiertlewski, M. (2006) A Compact Tactile Display for the Blind with Shape Memory Alloys. *IEEE International Conference on Robotics and Automation*, Orlando, FL, 15-19 May 2006, 3905-3910. https://doi.org/10.1109/ROBOT.2006.1642300

[21] Mansour, N.A., Fath El-Bab, A.M.R. and Abdellatif, M. (2012) Design of a Novel Multi-Modal Tactile Display Device for Biomedical Applications. 2012 *First International Conference on Innovative Engineering Systems*, Alexandria, 7-9 December 2012, 183-188. https://doi.org/10.1109/ICIES.2012.6530836

[22] Mohd Jani, J., Leary, M., Subic, A. and Gibson, M.A. (2014) A Review of Shape Memory Alloy Research, Applications and Opportunities. *Materials and Design*, **56**, pp. 1078-1113. https://doi.org/10.1016/j.matdes.2013.11.084

[23] Jayender, J., Patel, R.V., Nikumb, S. and Ostojic, M. (2005) Modelling and Gain Scheduled Control of Shape Memory Alloy Actuators. *Proceedings of the* 2005 *IEEE Conference on Control Applications*, Toronto, 28-31 August 2005, 767-772.

[24] Eisakhani, A., Ma, W., Gao, J., Culham, J.R. and Gorbet, R. (2011) Natural Convection Heat Transfer Modelling of Shape Memory Alloy Wire. *International Workshop Smart Materials*, *Structures & NDT in Aerospace Conference*, Montreal, 2-4 November 2011.

[25] Degeratu, S., Rotaru, P., Rizescu, S. and Bîzdoacă, N.G. (2013) Thermal Study of a Shape Memory Alloy (SMA) Spring Actuator Designed to Insure the Motion of a Barrier Structure. *Journal of Thermal Analysis and Calorimetry*, **111**, 1255-1262. https://doi.org/10.1007/s10973-012-2369-4

[26] Dynalloy Industries (2013) Technical Characteristics of Flexinol Actuator Wires. F1140 Rev J Datasheet. https://dynalloy.com/tech_sheets.php

[27] Kellogg's Research Labs (2020) Nitinol in Plain Language.

[28] Kumar, P.K. and Lagoudas, D.C. (2008) Introduction to Shape Memory Alloys. In: Lagoudas, D.C., Ed., *Shape Memory Alloys*, Vol. 1, Springer, Boston, MA, 1-51. https://doi.org/10.1007/978-0-387-47685-8_1

[29] Pissaloux, E.E. and Velazquez, R. (2012) Modelling and Temperature Control of Shape Memory Alloys with Fast Electrical Heating. *International Journal of Mechanics and Control*, **13**, 3-10.

[30] Tong, J., Mao, O. and Goldreich, D. (2013) Two-Point Orientation Discrimination versus the Traditional Two-Point Test for Tactile Spatial Acuity Assessment. *Frontiers in Human Neuroscience*, **7**, Article 579. https://doi.org/10.3389/fnhum.2013.00579